

This discussion paper is/has been under review for the journal Biogeosciences (BG).
Please refer to the corresponding final paper in BG if available.

Calcium carbonate corrosivity in an Alaskan inland sea

W. Evans^{1,2}, J. T. Mathis^{1,2}, and J. N. Cross^{1,2}

¹Ocean Acidification Research Center, School of Fisheries and Ocean Sciences, University of Alaska Fairbanks, Fairbanks, Alaska, USA

²National Oceanic and Atmospheric Administration, Pacific Marine Environmental Laboratory, Seattle, Washington, USA

Received: 26 August 2013 – Accepted: 5 September 2013 – Published: 10 September 2013

Correspondence to: W. Evans (wiley.evans@alaska.edu)

Published by Copernicus Publications on behalf of the European Geosciences Union.

BGD

10, 14887–14922, 2013

Calcium carbonate
corrosivity in an
Alaskan inland sea

W. Evans et al.

Title Page

Abstract

Introduction

Conclusions

References

Tables

Figures

⏪

⏩

◀

▶

Back

Close

Full Screen / Esc

Printer-friendly Version

Interactive Discussion



Abstract

Ocean acidification is the hydrogen ion increase caused by the oceanic uptake of anthropogenic CO_2 , and is a focal point in marine biogeochemistry, in part, because this chemical reaction reduces calcium carbonate (CaCO_3) saturation states (Ω) to levels that are corrosive (i.e. $\Omega \leq 1$) to shell-forming marine organisms. However, other processes can drive CaCO_3 corrosivity; specifically, the addition of tidewater glacial melt. Carbonate system data collected in May and September from 2009 through 2012 in Prince William Sound (PWS), a semi-enclosed inland sea located on the south-central coast of Alaska that is ringed with fjords containing tidewater glaciers, reveal the unique impact of glacial melt on CaCO_3 corrosivity. Initial limited sampling was expanded in September 2011 to span large portions of the western and central sound, and included two fjords proximal to tidewater glaciers: Icy Bay and Columbia Bay. The observed conditions in these fjords affected CaCO_3 corrosivity in the upper water column (< 50 m) in PWS in two ways: (1) as spring-time formation sites of mode water with near-corrosive Ω levels seen below the mixed layer across the sound, and (2) as point sources for surface plumes of glacial melt with corrosive Ω levels (Ω for aragonite and calcite down to 0.60 and 1.02, respectively) and carbon dioxide partial pressures ($p\text{CO}_2$) well below atmospheric levels. CaCO_3 corrosivity in glacial melt plumes is poorly reflected by $p\text{CO}_2$ or pH_T , indicating that either one of these carbonate parameters alone would fail to track Ω in PWS. The unique Ω and $p\text{CO}_2$ conditions in the glacial melt plumes enhances atmospheric CO_2 uptake, which, if not offset by mixing or primary productivity, would rapidly exacerbate CaCO_3 corrosivity in a positive feedback. The cumulative effects of glacial melt and air-sea gas exchange are likely responsible for the seasonal widespread reduction of Ω in PWS; making PWS highly sensitive to increasing atmospheric CO_2 and amplified CaCO_3 corrosivity.

BGD

10, 14887–14922, 2013

Calcium carbonate corrosivity in an Alaskan inland sea

W. Evans et al.

Title Page

Abstract

Introduction

Conclusions

References

Tables

Figures

◀

▶

◀

▶

Back

Close

Full Screen / Esc

Printer-friendly Version

Interactive Discussion



1 Introduction

The uptake of anthropogenic carbon dioxide (CO₂) by the contemporary ocean increases the concentration of hydrogen ions (lowers seawater pH), which drives a cascade of alterations in the marine carbonate system in a phenomenon known as ocean acidification (OA) (Gattuso and Hanssorn, 2011; Doney et al., 2009; Caldeira and Wickett, 2003; Raven et al., 2005; Orr et al., 2005; Dore et al., 2009). Of particular biogeochemical importance, raising hydrogen ion concentrations consume carbonate ions (CO₃²⁻), which in turn reduces the saturation state (Ω) of calcium carbonate (CaCO₃) minerals important for shell-forming marine organisms (Fabry et al., 2008; Feely et al., 2004; Feely et al., 2009; Millero, 2007). When Ω , defined as the ion product of CO₃²⁻ and calcium (Ca²⁺) in seawater relative to the stoichiometric solubility product for CaCO₃ at a given temperature, salinity and pressure, is reduced to levels below 1, waters become corrosive to CaCO₃ and dissolution occurs. Two major phases of CaCO₃, aragonite and calcite, have specific solubility products that cause aragonite to be ~ 1.5× more soluble than calcite (Dickson, 2010), such that aragonite becomes undersaturated and dissolves before calcite in the ocean (Orr et al., 2005). Corrosive Ω levels for both phases of CaCO₃ are naturally found in the ocean at depths below the level of continental shelves (Millero, 2007), however, ocean acidification as a direct response of rising atmospheric CO₂ is causing these levels to shoal above the depth of the shelf break (~ 200 m) and inundate shallow water in some coastal locations (Bryne et al., 2010; Mathis et al., 2011a; Bates et al., 2009; Feely et al., 2008, 2010; Leinweber and Gruber, 2013; Mathis et al., 2011b, 2014b) making these areas vulnerable to environmental changes with an associated disruption in ecosystem services (Cooley and Doney, 2009; Barton et al., 2012; Feely et al., 2012; Mathis et al., 2014a). In many of these locations, natural variability in the carbonate system and/or coastal eutrophication can combine synergistically with OA to drive manifestations of severe calcium carbonate corrosivity (Harris et al., 2012; Cai et al., 2011; Mathis et al., 2011b). However, independent of OA, CaCO₃ corrosivity can result from processes such as the

BGD

10, 14887–14922, 2013

Calcium carbonate corrosivity in an Alaskan inland sea

W. Evans et al.

Title Page

Abstract

Introduction

Conclusions

References

Tables

Figures



Back

Close

Full Screen / Esc

Printer-friendly Version

Interactive Discussion



influence of coastal rivers (Salisbury et al., 2008) and sea ice melt in high latitude settings (Yamamoto-Kawaii et al., 2009; Chierici and Fransson, 2009; Bates et al., 2009). To date, CaCO₃ corrosivity from direct glacial discharge has not been addressed.

Direct glacial discharge to the marine environment takes place at marine-terminating tidewater glaciers. The discharge at ocean/glacier interfaces has unique chemical characteristics free from additional alteration that would occur in proglacial (immediately in front of a glacier) streams draining mountain-terminating glaciers, which can add alkalinity to stream water via the dissolution of carbonate sediments and/or vegetation processes (Anderson et al., 2000). Direct glacial discharge from tidewater glaciers takes the form of melt plumes in adjacent, proglacial coastal waters, and are created by a mixture of subglacial discharge, melt from the glacier ice face, and melting calved ice (Motyka et al., 2003). Subglacial discharge, meaning it occurs at the grounding line of the glacier or at some other submarine level, can account for a high percentage (> 50 %) of the discharge from tidewater glaciers (Motyka et al., 2003; Walters et al., 1988; Mortensen et al., 2013). Subglacial discharge creates a region of turbulent convective flow immediately adjacent to the terminus of tidewater glaciers where mixing from rising buoyant melt plumes enhances melt from the glacier ice face, undercutting the glacier terminus and accelerating the calving rate (Motyka et al., 2003; Ritchie et al., 2008). The combination of these processes creates glacial melt plumes in proximal coastal waters with distinct temperature and salinity characteristics (Motyka et al., 2003; Walters et al., 1988; Mortensen et al., 2013).

Glacial melt plumes are expected to be biogeochemically unique, however, this has been under-represented in the literature. Studies have focused on the impact of glacial discharge from the standpoint of contributing to freshwater runoff (Neal et al., 2010), sea level rise (Arendt et al., 2002; Larsen et al., 2007; Gardner et al., 2013; Berthier et al., 2010), as a source of labile organic matter (Hood et al., 2009), as a source of stratification and/or turbidity that influences coastal primary productivity and carbon uptake (Dierssen et al., 2002; Shadwick et al., 2013), and as a source of the micronutrient iron (Bhatia et al., 2013). However, to our knowledge, there is virtually nothing in the current

BGD

10, 14887–14922, 2013

Calcium carbonate corrosivity in an Alaskan inland sea

W. Evans et al.

Title Page

Abstract

Introduction

Conclusions

References

Tables

Figures

◀

▶

◀

▶

Back

Close

Full Screen / Esc

Printer-friendly Version

Interactive Discussion



Calcium carbonate corrosivity in an Alaskan inland sea

W. Evans et al.

Title Page

Abstract

Introduction

Conclusions

References

Tables

Figures



Back

Close

Full Screen / Esc

Printer-friendly Version

Interactive Discussion



literature describing the impact of glacial melt on the marine carbonate system. To date a single study has reported undersaturated CO_2 partial pressures ($p\text{CO}_2$) with respect to the atmosphere in surface water impacted by glacial melt in Young Sound on the northeast coast of Greenland (Sejr et al., 2011). Sejr et al. (2011) observed a high sediment load in low- $p\text{CO}_2$ run-off from proglacial rivers draining the Greenland ice sheet, and a more than 100 μatm difference between directly measured $p\text{CO}_2$ and $p\text{CO}_2$ calculated from dissolved inorganic carbon (DIC) and total alkalinity (TA). The difference in $p\text{CO}_2$ was correlated to turbidity, with the largest disparity coinciding with instances of highest sediment load. The explanation invoked by Sejr et al. (2011) was that, due to the reactive nature of carbonate particles in glacial melt water (Brown, 2002), these particles reacted chemically either during storage or analysis of the DIC/TA samples, and added approximately 7 to 10 % more alkalinity, which then resulted in lower $p\text{CO}_2$ than what was directly observed. Sejr et al. (2011) hypothesized that the low- $p\text{CO}_2$ glacial melt, which contained reactive particles that would consume additional CO_2 , contributed to the widespread low surface $p\text{CO}_2$ seen throughout Young Sound. It follows that direct glacial discharge less buffered by high concentrations of reactive particles derived from river sediments should drive severe CaCO_3 corrosivity in addition to undersaturated $p\text{CO}_2$. Here, we present data from Prince William Sound (PWS), an Alaskan inland sea ringed with tidewater glaciers (Fig. 1), which show direct glacial melt has a radical impact on the corrosivity of CaCO_3 in this high latitude coastal setting.

2 Study area

PWS is a semi-enclosed, sub-arctic inland sea on the south-central coast of Alaska that exchanges with the adjacent Gulf of Alaska (GOA) largely via two passages: Hinchinbrook Entrance and Montague Strait (Fig. 1). It is defined as an inland sea because appreciable horizontal circulation occurs in the surface layer (Niebauer et al., 1994; Musgrave et al., 2013; Halverson et al., 2012b; Vaughan et al., 2001). Downwelling-favorable winds, which dominate from September through May, drive surface flow into

**Calcium carbonate
corrosivity in an
Alaskan inland sea**

W. Evans et al.

[Title Page](#)[Abstract](#)[Introduction](#)[Conclusions](#)[References](#)[Tables](#)[Figures](#)[Back](#)[Close](#)[Full Screen / Esc](#)[Printer-friendly Version](#)[Interactive Discussion](#)

PWS through Hinchinbrook Entrance, with compensatory outflow through Montague Strait (Niebauer et al., 1994; Halverson et al., 2012a). This “flow-through” scenario is reduced and more complex between May and September, when winds are only weakly downwelling favorable or upwelling favorable and surface flows are typically weaker with reversals through either strait becoming more common (Halverson et al., 2012a; Niebauer et al., 1994). However, transport at this time can be highly baroclinic, with inflow at depth flushing the deepest portions of PWS (> 400 m) in as fast as a month (Halverson et al., 2012a). The central region of PWS is a deep 400 m basin, which is silled from the adjacent GOA at a depth of approximately 250 m at Hinchinbrook Entrance and near 150 m at Montague Strait (Fig. 1). The central region is defined as the area north of Hinchinbrook Entrance, and is approximately 50 km wide. A shoal with a series of islands separates the western and central regions of PWS, and the main north-south channel in western PWS is Knight Island Passage (K.I.P.; Fig. 1). Near the northern terminus of K.I.P. is the deepest area in PWS, with depths reaching approximately 700 m. Surrounding PWS are the Chugach and Kenai Mountain ranges to the north and west, respectively, which reach to heights approaching 4 km. These mountain ranges contain extensive ice fields and glaciers, many of which are losing volume rapidly due to climate change (Arendt et al., 2002, 2006). Encircling PWS from Columbia Bay westward are numerous proglacial fjords with tidewater glaciers originating from these mountains (Fig. 1). Glacial runoff, either as a direct input to the sound or indirectly via proglacial streams, contributes an estimated 60 % of the freshwater discharged to PWS, which itself contributes 11 % of the total runoff to the GOA (Neal et al., 2010). The large freshwater supply to PWS, coupled with the fact that the adjacent GOA shelf is shallower than significant portions of the sound, also makes this inland sea a complex fjord-type estuary.

3 Data collection and analysis

Beginning in 2009, bi-annual carbonate system measurements were collected within PWS during May and September as part of a broader carbonate system study on the GOA continental margin (Mathis et al., 2014b; Evans and Mathis, 2013; Evans et al., 2013b). Data were collected aboard the US Fish and Wildlife Service R/V *Tiglax*. Hydrographic data and seawater samples were collected from select depths at stations in PWS using a rosette equipped with 5-L Niskin bottles and a Sea-Bird 911Plus conductivity-temperature-depth (CTD) profiler. Temperature (T) and salinity (S ; calculated from conductivity) data presented here were processed using standard protocols recommended by Seabird, and salinity data are reported in this manuscript using the Practical Salinity Scale (PSS-78, dimensionless). DIC and TA samples were drawn from Niskin bottles into clean 250 mL Pyrex glass reagent bottles using established gas sampling protocols (Dickson et al., 2007). The Pyrex bottles were pretreated with 200 μL of saturated HgCl_2 solution to prohibit biological alteration, and a headspace of $< 1\%$ of the bottle volume was left to allow for water expansion. Fixed samples were sealed and analyzed for DIC and TA at the University of Alaska (UAF) Ocean Acidification Research Center (OARC) using a VINDTA 3C (<http://www.marianda.com/index.php?site=products&subsite=vindta3c>). Seawater certified reference materials (prepared by A. G. Dickson, Scripps Institute of Oceanography) were analyzed before samples were processed to ensure that DIC and TA measurements were accurate to within 0.1% ($\sim 2 \mu\text{mol kg}^{-1}$). Nutrient samples were drawn from Niskin bottles into 20 mL Nalgene high density polyethylene scintillation vials, frozen at sea and processed at UAF using a Alpkem Rapid Flow Analyzer 300 and protocols following (Whitledge et al., 1981). The nominal precision and accuracy of the silicate and phosphate measurements were $< 0.1 \mu\text{mol kg}^{-1}$. The saturation state of aragonite (Ω_{arag}) and calcite (Ω_{calc}) phases of CaCO_3 were calculated using the T , S , pressure, DIC, TA, silicate and phosphate data with the constants described by Lueker et al. (2000) via a Matlab version of CO2SYS (van Heuven et al., 2011). The Lueker

Title Page

Abstract

Introduction

Conclusions

References

Tables

Figures



Back

Close

Full Screen / Esc

Printer-friendly Version

Interactive Discussion



et al. (2000) constants were chosen because they are applicable to measurements over the range of T and S values observed in PWS, and, with these constants, pH is calculated on the total hydrogen ion scale (pH_T).

4 Results

5 A total of 8 cruises surveyed PWS between 2009 and 2012 during May and September (Fig. 1). The first 5 cruises conducted a limited number of stations within Montague Strait and K.I.P. in western PWS. The three latter cruises in this dataset, first occurring in September 2011, had expanded coverage over western and central portions of PWS, during which 56% of the 744 carbonate system measurements were collected. One station, located near the northern terminus of K.I.P, was sampled during all 8 cruises (circled station in Fig. 1). During September 2011, water column carbonate chemistry was sampled for the first time at a station in Icy Bay adjacent to the Chenega Glacier (within 1 km; Fig. 1). The following May, a station was occupied in Columbia Bay abutting the moraine shoal of Columbia Glacier. The depth of the moraine shoal ranges between near sea level to ~ 20 m, and it acts as a barrier to ship travel because it is populated with grounded icebergs produced by the calving face of Columbia Glacier. The terminus of Columbia Glacier was approximately 20 km north of the moraine shoal at the time the survey was conducted (http://earthobservatory.nasa.gov/Features/WorldOfChange/columbia_glacier.php). In 10
15
20
25
September 2012 both near-glacier sites were repeated, however our approach to Chenega Glacier in Icy Bay was limited by extensive calved ice. General patterns immediately evident in the PWS dataset were: (1) variability in all parameters was greatest at the surface (< 9 m) compared with that seen at depth (> 500 m), and (2) there was a significant increase in the dynamic range of surface T , S , TA, DIC, Ω_{arag} and Ω_{calc} in September relative to May, which was not reflected in pCO_2 or pH_T (Table 1).

The trends in carbonate parameters versus salinity for the entire PWS dataset revealed a change in the relationship between Ω_{arag} , pCO_2 and pH_T across the contin-

BGD

10, 14887–14922, 2013

Calcium carbonate corrosivity in an Alaskan inland sea

W. Evans et al.

Title Page

Abstract

Introduction

Conclusions

References

Tables

Figures

◀

▶

◀

▶

Back

Close

Full Screen / Esc

Printer-friendly Version

Interactive Discussion



uum of observed salinities (Fig. 2). Figure 2 shows these trends relative to the TA/DIC ratio, providing a means for identifying instances of DIC addition or removal relative to TA; and when TA and DIC are close to 1, the concentration of CO_3^{2-} is low (Chierici and Fransson, 2009; Sarmiento and Gruber, 2006). Mean deep water (> 500 m) TA and DIC were not largely different between May and September, with concentrations near 2220 and 2160, respectively (Table 1). The lowest TA/DIC ratios were in this water with values of 1.01 (Table 1). The high DIC relative to TA in deep water was presumed to result from the remineralization of organic matter that was produced in the euphotic zone and delivered to depth, and from the seasonal exchange of deep water with the adjacent GOA (Niebauer et al., 1994) that has a low TA/DIC ratio (Mathis and Evans, unpublished data). Ω_{arag} , $p\text{CO}_2$ and pH_T are tightly coupled in this deep water, with corrosive levels of Ω_{arag} (i.e. < 1) coinciding with values of pH_T below 7.87 and $p\text{CO}_2$ above $565 \mu\text{atm}$ (Fig. 2). These carbonate parameters are also tightly coupled between salinities of 24 and 32, as instances of high TA/DIC ratio (> 1.1), which correspond to surface (< 9 m) measurements (Table 1), coincided with the highest values of Ω_{arag} and pH_T , and $p\text{CO}_2$ well below saturation with respect to the atmosphere (Fig. 2). The instances of high TA/DIC ratio were presumably caused by episodes of high primary productivity, and this assumption was supported by limited ΔO_2 measurements (i.e. measured minus saturation values of O_2) that show simultaneous levels of oversaturation approaching $+100 \mu\text{mol kg}^{-1}$ in high TA/DIC ratio water (data not shown) that, in the face of rapid air-sea exchange, could have only resulted from high rates of primary production. In both of the above situations, Ω_{arag} and pH_T tracked each other while $p\text{CO}_2$ had an inverse trend, and these relationships between the three variables are typical of the manifestations of CaCO_3 corrosivity in coastal settings (Feely et al., 2008; Harris et al., 2013; Cai et al., 2011; Leinweber and Gruber, 2013; Mathis et al., 2013). However, these relationships between Ω_{arag} , pH_T and $p\text{CO}_2$ became decoupled at salinities less than 24 in this setting (Fig. 2). In these low-salinity surface waters, TA was diluted to concentrations near and less than $1700 \mu\text{mol kg}^{-1}$, and the TA/DIC ratio approached the low levels seen in PWS deep basin water (Table 1). Due to this pairing

**Calcium carbonate
corrosivity in an
Alaskan inland sea**

W. Evans et al.

Title Page

Abstract

Introduction

Conclusions

References

Tables

Figures

◀

▶

◀

▶

Back

Close

Full Screen / Esc

Printer-friendly Version

Interactive Discussion



of chemical conditions, corrosive levels of Ω_{arag} at the lowest salinities were similar to those seen at the highest salinities, however, $p\text{CO}_2$ was undersaturated with respect to the atmosphere while pH_T was not as low as the values observed in deep water (Fig. 2). In this setting, pH_T or $p\text{CO}_2$ alone would fail to represent the corrosivity of low salinity surface water.

The decoupling between CaCO_3 corrosivity and $p\text{CO}_2$ or pH_T in PWS appeared in September but not May. May Ω_{arag} data followed a predictable relationship with $p\text{CO}_2$ that was well represented by a polynomial fit (Fig. 3). High $p\text{CO}_2$ levels coincided with low and corrosive Ω_{arag} values, and lowest $p\text{CO}_2$ corresponded to highest Ω_{arag} . Lowest $p\text{CO}_2$ and highest Ω_{arag} conditions were seen at this time. The relationship between Ω_{arag} and $p\text{CO}_2$ was far less predictable for September data. September data, in general, followed a different trajectory than the May data, being mostly above the May polynomial fit at $p\text{CO}_2$ values less than $600 \mu\text{atm}$, and with a large degree of scatter at a $p\text{CO}_2$ range between 200 and $400 \mu\text{atm}$ (Fig. 3). September data falling above the May fit with high $p\text{CO}_2$ for a given Ω_{arag} were likely the result of the seasonal surface warming seen in PWS between May and September, as the observed mean 5°C temperature increase would drive a $60 \mu\text{atm}$ increase in $p\text{CO}_2$ but only a 0.05 unit increase in Ω_{arag} relative to the spring mean surface values (Table 1). The largest variability in Ω_{arag} at a given $p\text{CO}_2$ in the September data coincided with episodes of depleted CO_3^{2-} concentrations by as much as $100 \mu\text{mol kg}^{-1}$ (Fig. 3). The lowest September Ω_{arag} value observed (0.06) was one of the low- $p\text{CO}_2$, low- CO_3^{2-} data points, and was seen in a surface water sample diluted in TA (Fig. 2); this surface sample was collected adjacent to the Chenega Glacier in Icy Bay (Figs. 1 and 4).

During each September occupation of a station proximal to Chenega Glacier in Icy Bay (Fig. 1), cold, low- σ_t (potential density anomaly) surface water was observed with undersaturated $p\text{CO}_2$ and Ω_{arag} (Fig. 4). These surface plumes have low salinity, are diluted in TA, and have low TA/DIC ratios making them depleted in CO_3^{2-} . The first observation of surface near-corrosive calcite saturations in the GOA was at this site and under these conditions (Fig. 4). However, our data reveal that there is apprecia-

Calcium carbonate corrosivity in an Alaskan inland sea

W. Evans et al.

Title Page

Abstract

Introduction

Conclusions

References

Tables

Figures

◀

▶

◀

▶

Back

Close

Full Screen / Esc

Printer-friendly Version

Interactive Discussion



**Calcium carbonate
corrosivity in an
Alaskan inland sea**

W. Evans et al.

[Title Page](#)[Abstract](#)[Introduction](#)[Conclusions](#)[References](#)[Tables](#)[Figures](#)[⏪](#)[⏩](#)[◀](#)[▶](#)[Back](#)[Close](#)[Full Screen / Esc](#)[Printer-friendly Version](#)[Interactive Discussion](#)

ble variability in the surface expressions of CaCO_3 corrosivity in glacial melt plumes. A consistent feature of the water column in and around Icy Bay at this time of year was a mid-depth temperature maximum, which is caused by the cold surface plume over-riding warmer water from the adjacent main basin of western PWS (Gay III and Vaughan, 2001). During 2011, the temperature of this layer was $\sim 3^\circ\text{C}$ warmer than it was in 2012; Ω_{arag} in this layer, and at the surface, was nearly 0.3 units higher in 2011 than in 2012 (Fig. 4). To evaluate the source waters responsible for these characteristics, we calculated mixing lines, following Walters et al. (1988), between: (1) PWS source waters in the mid-depth temperature maximum and freshwater at 0°C (Fig. 5; “mixing line”), and (2) PWS source water and water from glacial melt (Fig. 5; “melt-line”). When ice, either at or calved from the glacier terminus, melts in seawater, latent heat of fusion causes a relatively large change in temperature per unit salinity. This trait has been used to distinguish glacial melt from other sources of freshwater in Columbia Bay (Walters et al., 1988) and in some Greenland fjords (Mortensen et al., 2013). The larger change in temperature per unit salinity results in a steeper “melt line” from adding glacial melt compared with the “mixing line” from freshwater addition. Note that subglacial discharge alone would simply be a source of freshwater, albeit does not typically occur alone in summer but rather in conjunction with melting from the glacier ice face that then enhances the calving rate from the glacier (Ritchie et al., 2008; Motyka et al., 2003). As such, glacial melt plumes at this time of year would be a combination of these three constituents of glacial melt. T/S data collected during 2012 track the “melt line” indicated strong modification by glacial melt, with only a small region of departure in the very near surface layer (Figs. 4 and 5). The data from 2011 follow a near-consistent trajectory between the “mixing line” and the “melt line”, indicating only moderate modification by glacial melt relative to the 2012 data (Fig. 5). We suggest that the more corrosive conditions observed in 2012 were due to the greater addition of glacial melt compared with that seen in 2011. Ancillary evidence that the degree of glacier melt in Icy Bay was greater in 2012 is that our approach was limited to at least 3 km from the terminus of Chenega Glacier (Fig. 1) by the high density of

calved ice, but the most corrosive conditions to date were observed then. In 2011 we were able to get much closer to the glacier terminus yet the water column was less corrosive to CaCO_3 (Fig. 4)

Data from Icy Bay illustrated that there are year-to-year differences in glacial melt and the degree of CaCO_3 corrosivity, but data from Columbia Bay show that there is a critical seasonal difference that has implications for corrosivity over the upper water column in PWS. In May and September 2012, a station near the moraine shoal of Columbia Bay (Fig. 1) was sampled for carbonate chemistry. Profiles revealed vastly different conditions between these months in this fjord (Fig. 6). During September, the mid-depth temperature maximum indicative of the adjacent PWS basin water was present, as well as a cold, low- σ_t surface layer with Ω_{arag} levels less than those seen at mid-depth. Although there are differences between these September data, and those from Icy Bay (Fig. 4), the patterns are consistent between the two fjords and reflect the varying degree of corrosivity in surface plume water. Conversely, in May, there was essentially no plume. Vertical profiles of T and σ_t show nearly homogenous conditions with very little evidence of stratification (Fig. 6). A slight decrease in σ_t at the surface was evident and implied a minor presence of low-salinity water, and temperatures cooled considerably from depth to the surface. Ω_{arag} at this time varied by only ± 0.1 units, being near-corrosive with values close to 1.2 throughout the water column (Fig. 6). At adjacent stations, we identified a water mass at 40 m that appeared to extend from Columbia Bay across a large portion of western PWS (Fig. 7). This mode water had specific T and σ_t characteristics, and was below the mixed layer based on the World Ocean Circulation Experiment mixed layer depth criterion of 0.125 kg m^{-3} (Monterey and Levitus, 1997). This water mass could also be identified by mid-depth temperature minima in the broader PWS (Fig. 7), and such cold layers have been previously observed in association with proglacial fjords (Gay III and Vaughan, 2001; Pickard, 1967). We suggest that Columbia Bay, and likely other proglacial fjords in and around PWS, serve as mode water formation sites near the end of winter when surface water temperatures are at their coolest. Glacial melt at this time is typically at a

BGD

10, 14887–14922, 2013

Calcium carbonate corrosivity in an Alaskan inland sea

W. Evans et al.

Title Page

Abstract

Introduction

Conclusions

References

Tables

Figures

◀

▶

◀

▶

Back

Close

Full Screen / Esc

Printer-friendly Version

Interactive Discussion



5 minimum because subglacial discharge is reduced and proximal fjord water temperatures are cooler (Motyka et al., 2003), however, for the case of Columbia Glacier, which has been retreating catastrophically (Post et al., 2011), the proximal fjord is likely still impacted by melt sources from the glacier that then can affect water properties on the seaward side of the moraine shoal in Columbia Bay. Thus, at its formation site, this mode water may be imprinted with chemical signals from glacial melt. In this way mid-layers of the water column may be impacted by corrosive mode water formed in proglacial fjords, while the surface water column during this time period serves as a refuge from CaCO_3 corrosivity.

10 Data collected at PWS2, the station north of K.I.P. that has been repeated during every cruise in PWS (Fig. 1), revealed that springtime temperature minima occur every year. The magnitudes vary, however, and these features aren't always directly associated with local minima in Ω_{arag} (Fig. 8). From the limited number of profiles done in PWS thus far, it is not possible to diagnose the source of chemical variability across mid-depth temperature minima, however, we can speculate that it is related to: (1) year-to-year variability at the formation sites within proglacial fjords, (2) variability across potential mode water formation sites, and (3) variable connectivity between the adjacent GOA and PWS. The single May profile in a glaciated fjord prevents any kind of assessment of the first two potential sources of variability, and clearly more data are needed to address these points. However, PWS2 data does provide a hint of the variable connectivity between the adjacent GOA and PWS. For instance, calcite undersaturation was observed in the deep basin water north of K.I.P. during spring (Table 1, Figs. 2 and 3). This observation has only been made once, and we speculate that this is related to the synchronicity between when our measurements were collected and when downwelling conditions abated on the shelf. Being that deep water renewal events occur during non-downwelling periods (Niebauer et al., 1994) and can flush bottom waters in as rapidly as a month (Halverson et al., 2012a), calcite undersaturation could build up during stagnant winter months in the deepest portions of PWS but be extinguished by the time our survey takes place in May given this is the time seasonal downwelling

Calcium carbonate corrosivity in an Alaskan inland sea

W. Evans et al.

[Title Page](#)[Abstract](#)[Introduction](#)[Conclusions](#)[References](#)[Tables](#)[Figures](#)[Back](#)[Close](#)[Full Screen / Esc](#)[Printer-friendly Version](#)[Interactive Discussion](#)

Calcium carbonate corrosivity in an Alaskan inland sea

W. Evans et al.

Title Page

Abstract

Introduction

Conclusions

References

Tables

Figures

⏪

⏩

◀

▶

Back

Close

Full Screen / Esc

Printer-friendly Version

Interactive Discussion



conditions are on the decline (Mathis et al., 2014b; Weingartner, 2007). Year-to-year differences in downwelling forcing on the shelf can be large (Mathis et al., 2014b), and likely determine if calcite undersaturation is observed given our set cruise schedule. Analogously, variability in the mid-depth temperature minima is likely a function of when our measurements were made relative to the conditions in PWS at the time. These temperature minima are ephemeral, lasting possibly only a few months (see Fig. 4 in Gay III and Vaughan, 2001), and have not been observed during September at PWS2 (Fig. 8).

The cumulative pulse of corrosive melt plumes from proglacial fjords in late summer/early autumn may play a large role in the wholesale reduction in CaCO_3 saturations in PWS. Surface Ω_{arag} values at PWS2 are lower in September than they are in May (Fig. 8 and Table 1); areal mean September CaCO_3 saturations are $\sim 20\%$ lower than those in May, and coincide with a 13% reduction in TA (Table 1). At this time, the dynamic range of TA and DIC increase by 85% and 67%, respectively (Table 1), likely due to some combination of direct glacial melt and other sources of runoff. With the current dataset, it is not possible to partition glacial melt versus other sources of freshwater. However, given the evidence described above, we expect direct glacial discharge plays a large role in setting the seasonal increase in CaCO_3 corrosivity within PWS. Note that the lesser increase in the dynamic range of DIC relative to TA suggests that a process is adding DIC with little effect on TA, and is at play during the period of greatest CaCO_3 corrosivity.

5 Discussion

A critical result of this work applicable to any coastal setting impacted by glacial melt is that CaCO_3 corrosivity is poorly reflected by $p\text{CO}_2$ or pH_T alone, indicating that either one of these carbonate parameters in isolation would fail to track corrosive conditions in these settings. This is not the case for the manifestation of CaCO_3 corrosivity in coastal upwelling regions (Feely et al., 2008; Harris et al., 2013) or in areas impacted

Calcium carbonate corrosivity in an Alaskan inland sea

W. Evans et al.

Title Page

Abstract

Introduction

Conclusions

References

Tables

Figures

◀

▶

◀

▶

Back

Close

Full Screen / Esc

Printer-friendly Version

Interactive Discussion



by rivers (Salisbury et al., 2008; Cai et al., 2011; Evans et al., 2013a; Feely et al., 2012) that experience high $p\text{CO}_2$. This realization is essential for the establishment of robust monitoring efforts targeting OA in proglacial coastal settings. The approach of Mathis et al. (2013) to employ empirical relationships between $p\text{CO}_2$ and Ω_{arag} in order to track

5 CaCO_3 corrosivity in bottom waters on the Bering Sea shelf would fall short in this setting because of the decoupling of these parameters in regions impacted by glacial melt plumes. Although untested in proglacial fjords, the multiple linear regressions (MLR) developed by Evans et al. (2013b) should fair better as those predict both TA and DIC, thereby accounting for the non-linearity of the carbonate system that provokes the variability in Ω at low $p\text{CO}_2$ levels (Fig. 3); however, because the relationship between

10 nitrate (NO_3^-) and DIC in glacial melt water is uncertain, and the MLR's used by Evans et al. (2013b) are heavily based on NO_3^- , we expect large error in the predictions using those equations. Only the direct measurement of two carbonate parameters will allow Ω_{arag} to be accurately quantified in settings where glacial melt plumes are encountered.

15 CaCO_3 corrosivity caused by the addition of direct glacial melt is not OA; that is, acidification by atmospheric CO_2 uptake. However, the undersaturated $p\text{CO}_2$ and Ω_{arag} levels in glacial melt plumes can cause a feedback that further decreases Ω_{arag} levels via air-sea CO_2 exchange. This is not the case for sea ice melt, which is typically oversaturated in $p\text{CO}_2$ with respect to the atmosphere (Miller et al., 2011; Bates et al.,

20 2009), even though it too is a source of CaCO_3 corrosivity to the ocean (Yamamoto-Kawai et al., 2009; Mathis et al., 2011b). Undersaturated $p\text{CO}_2$ with respect to the atmosphere in glacial melt plumes would enhance atmospheric CO_2 uptake, and the resultant change in DIC from this exchange can be estimated assuming complete equilibration of the melt plume with the atmosphere. This estimation invokes the Revelle factor, which describes the sensitivity of $p\text{CO}_2$ to changes in DIC (Sarmiento and Gruber, 2006; Takahashi et al., 1993). The change in DIC from air-sea gas exchange (ΔDIC) can be determined by manipulating the Revelle factor definition by Sundquist et al. (1979): $\Delta\text{DIC} = \Delta p\text{CO}_2 / p\text{CO}_{2,\text{SW}} / \text{Revelle factor} \times \text{DIC}$. ΔDIC can then be equated to a change in Ω_{arag} given the initial TA, DIC, T and S properties. For the case of

25

autumn 2012 Icy Bay surface water, the air minus sea $p\text{CO}_2$ ($\Delta p\text{CO}_2$) was $85 \mu\text{atm}$, seawater $p\text{CO}_2$ ($p\text{CO}_{2,\text{SW}}$) was $295 \mu\text{atm}$, DIC was $1237 \mu\text{mol kg}^{-1}$, and the Revelle factor was 18. This equates to a $20 \mu\text{mol kg}^{-1}$ increase in DIC via atmospheric CO_2 uptake, and a 0.5 unit decrease in Ω_{arag} from the observed already undersaturated conditions (Fig. 4). Assuming the glacial melt plume spans 10 m of the upper water column and an average September sea-air CO_2 flux of $10 \text{ mmol CO}_2 \text{ m}^{-2} \text{ d}^{-1}$ following Evans and Mathis (2013), this change in Ω_{arag} could occur in as rapidly as 20 days.

The above example calculation can be depicted graphically for combinations of water properties mixed linearly between autumn 2012 Icy Bay surface water ($\text{TA} = 1285 \mu\text{mol kg}^{-1}$, $T = 6.4^\circ\text{C}$, $S = 18$) and a approximation of TA ($430 \mu\text{mol kg}^{-1}$), T (0°C), and S (0) properties in glacial melt using published data from the nearby land-terminating Bench Glacier (Anderson et al., 2000). The top panel of Fig. 9 shows the $p\text{CO}_2$, Ω_{arag} , and Revelle factor responses to mixing these two water masses linearly along the salinity gradient from 0 to 18 for different cases of TA/DIC ratio ranging from 1.15 to 1.00. This range of TA/DIC ratios brackets the highest and lowest values observed in the PWS data set (Table 1), and produces an envelop of trajectories for $p\text{CO}_2$, Ω_{arag} , and Revelle factor values that result from mixing across the continuum between Bench Glacier and Icy Bay waters. This calculation shows that the TA/DIC ratio of Icy Bay water sets whether coincidentally undersaturated $p\text{CO}_2$ and Ω_{arag} will be observed, and that the Revelle factor is highest in the lowest TA/DIC ratio water. The lower panel of Fig. 9 illustrates the potential change in Ω_{arag} ($\Delta\Omega_{\text{arag}}$) that would ensue given these $p\text{CO}_2$, DIC and Revelle factor conditions. $\Delta\Omega_{\text{arag}}$ will have no change or be positive only when surface water $p\text{CO}_2$ is near or above saturation with the atmosphere, or when Ω_{arag} is already near zero. In all other cases, acidification by atmospheric CO_2 uptake will intensify CaCO_3 corrosivity in glacial melt plumes. These calculations only take into account air-sea CO_2 exchange, however, the time rate of change for $p\text{CO}_2$ and Ω are both also dependent on warming, mixing and biological processes. True trajectories of the evolution of $p\text{CO}_2$ and Ω in glacial melt plumes fall somewhere within the envelopes depicted in Fig. 9, and are essential to resolve in order to make robust

BGD

10, 14887–14922, 2013

Calcium carbonate corrosivity in an Alaskan inland sea

W. Evans et al.

Title Page

Abstract

Introduction

Conclusions

References

Tables

Figures

◀

▶

◀

▶

Back

Close

Full Screen / Esc

Printer-friendly Version

Interactive Discussion



Calcium carbonate corrosivity in an Alaskan inland sea

W. Evans et al.

Title Page

Abstract

Introduction

Conclusions

References

Tables

Figures

◀

▶

◀

▶

Back

Close

Full Screen / Esc

Printer-friendly Version

Interactive Discussion



5 predictions of the downstream impact of glacial melt addition. Corrosive melt plumes increase in corrosivity via air-sea gas exchange, and will impart their corrosivity on adjacent coastal water through mixing. We posit that the interaction between glacial melt plumes and air-sea CO_2 exchange is the likely candidate to explain the disparity between the changes in TA and DIC dynamic ranges between May and September, and the wholesale seasonal reduction of Ω in PWS (Table 1). Further study should evaluate the evolution of the coupled roles of glacial melt addition and atmospheric CO_2 uptake in driving this change in CaCO_3 corrosivity. We anticipate these processes combine to have a large impact regionally with PWS, which also affects the adjacent continental margin.

10 CaCO_3 corrosivity from direct glacial melt impacts the upper 50 m of the water column of PWS in two ways: (1) as mode waters with distinct chemical signals, and (2) as surface plumes of glacial melt. These are seasonally distinct signals imply a transition from a refugium from CaCO_3 corrosivity for surface-dwelling organisms in May to a more corrosive surface environment in September. The opposite would be the case for sub-surface waters influenced by mode waters formed in proglacial fjords, with corrosivity there reduced in September as opposed to May. The downstream extent of mode waters emanating from proglacial fjords is uncertain, and likely impacts a narrow range of the water column over relatively short distances. However, ribbons of corrosive mode water extending from proglacial fjords can be sources of the large mid-depth variability, as observed by Evans et al. (2013b) on the GOA continental margin, with potential consequences for vertical migrating organisms in the water column. On the contrary to this local impact, the seasonal increase of CaCO_3 corrosivity in the PWS surface layer may have farther-reaching effects. During the non-downwelling period of the year, the “flow-through” scenario seen in PWS is far less distinct (Niebauer et al., 1994; Halverson et al., 2012a) due to the constricted nature of this inland sea combined with reduced downwelling-favorable winds, and concomitant with this is the seasonal increase in CaCO_3 corrosivity. When downwelling-favorable winds increase in September, the corrosive surface water that has built up in PWS would be rapidly evacuated.

uated to the continental shelf. This pulse of CaCO_3 corrosivity would become integrated into the poleward, alongshore-flowing Alaska Coastal Current, and impact ecosystems downstream. Cruise data collected thus far have not resolved this potential pulse of corrosivity to the continental margin from the PWS.

6 Summary

We have presented a growing dataset of carbonate system measurements collected within PWS, a semi-enclosed inland sea on the south-central coast of Alaska. These data revealed that conditions corrosive to CaCO_3 evolve through the influence of direct glacial discharge in a seasonally dependent manner: as near-corrosive mode water emanating for proglacial fjords, and as glacial melt plumes. CaCO_3 corrosivity was most intense in glacial melt plumes proximal to the terminal face of the Chenega tide-water glacier in Icy Bay. This plume water was undersaturated with respect to both aragonite (and nearly so for calcite) and atmospheric $p\text{CO}_2$. Simultaneous undersaturation of Ω_{arag} and $p\text{CO}_2$ sets up the condition whereby air-sea gas exchange can exacerbate CaCO_3 corrosivity by increasing DIC. This situation is unique to environments influenced by glacial melt plumes, and demonstrates that $p\text{CO}_2$ or pH_T alone would fail to capture manifestations of CaCO_3 corrosivity in these regions. We speculate that the cumulative impact of glacial melt plumes acts in concert with atmospheric CO_2 uptake to drive a wholesale reduction in Ω during September relative to May when surface melt plumes are non-existent. This is a seasonally modulated process that is likely terminated at the start of downwelling season when PWS functions in more of a “flow through” manner, evacuating a pulse of corrosive surface water to the adjacent GOA continental margin. The addition of glacial melt to PWS, combined with its semi-confined circulation pattern during the melt season, make it susceptible to significantly amplified corrosivity due to increasing atmospheric CO_2 . The link between the addition of corrosive glacial melt and air-sea gas exchange should be further studied as this potentially plays a significant role in shaping ecosystems both within PWS and in areas

Calcium carbonate corrosivity in an Alaskan inland sea

W. Evans et al.

Title Page

Abstract

Introduction

Conclusions

References

Tables

Figures

◀

▶

◀

▶

Back

Close

Full Screen / Esc

Printer-friendly Version

Interactive Discussion



downstream along the coast of Alaska that would be affected by the autumn release of corrosive surface waters.

Acknowledgements. We are grateful to Captain Billy Pepper and the crew of the US Fish and Wildlife Service R/V *Tiglux* for their help and support of our work in Prince William Sound. We express gratitude toward Natalie Monacci, Dan Naber, Stacey Reisdorph and Kristen Shake for their help with data collection and sample processing, and Molly McCammon for her continued support of ocean acidification research in Alaska. This work was funded by the Alaska Ocean Observing System under NOAA awards A08NOS4730406 and NA11NOS0120020, the National Science Foundation (PLR-1107997) and the NOAA Ocean Acidification Program.

References

- Anderson, S. P., Drever, J. I., Frost, C. D., and Holder, P.: Chemical weathering in the foreland of a retreating glacier, *Geochimica et Cosmochimica Acta*, 64, 1173–1189, 2000.
- Arendt, A., Echelmeyer, K. A., Harrison, W., Lingle, C., Zirnheld, S., Valentine, V., Ritchie, B., and Druckenmiller, M.: Updated estimates of glacier volume changes in the western Chugach Mountains, Alaska, and a comparison of regional extrapolation methods, *J. Geophys. Res.*, 111, 1–12, 2006.
- Arendt, A. A., Echelmeyer, K. A., Harrison, W. D., Lingle, C. S., and Valentine, V. B.: Rapid Wastage of Alaska Glaciers and Their Contribution to Rising Sea Level, *Science*, 297, 382–386, 2002.
- Barton, A., Hales, B., Waldbusser, G., Langdon, C., and Feely, R. A.: The Pacific oyster, *Crassostrea gigas*, shows negative correlation to naturally elevated carbon dioxide levels: Implications for near-term ocean acidification effects, *Limnol. Oceanogr.*, 57, 698–710, 2012.
- Bates, N. R., Mathis, J. T., and Cooper, L. W.: Ocean acidification and biologically induced seasonality of carbonate mineral saturation states in the western Arctic Ocean, *J. Geophys. Res.*, 114, doi:10.1029/2008JC004862, 2009.
- Berthier, E., Schiefer, E., Clarke, G. K. C., Menounos, B., and Rémy, F.: Contribution of Alaskan glaciers to sea-level rise derived from satellite imagery, *Nature Geosci.*, 3, 92–95, doi:10.1038/NGE0737, 2010.

BGD

10, 14887–14922, 2013

Calcium carbonate corrosivity in an Alaskan inland sea

W. Evans et al.

Title Page

Abstract

Introduction

Conclusions

References

Tables

Figures

◀

▶

◀

▶

Back

Close

Full Screen / Esc

Printer-friendly Version

Interactive Discussion



**Calcium carbonate
corrosivity in an
Alaskan inland sea**

W. Evans et al.

Title Page

Abstract

Introduction

Conclusions

References

Tables

Figures

◀

▶

◀

▶

Back

Close

Full Screen / Esc

Printer-friendly Version

Interactive Discussion



Bhatia, M. P., Kujawinski, E. B., Das, S. B., Breier, C. F., Henderson, P. B., and Charette, M. A.: Greenland meltwater as a significant and potentially bioavailable source of iron to the ocean, *Nature Geosci.*, 6, 2013.

Brown, G. H.: Glacier meltwater hydrochemistry, *Appl. Geochem.*, 17, 855–883, 2002.

5 Bryne, R. H., Mecking, S., Feely, R. A., and Liu, X.: Direct observations of basin-wide acidification on the North Pacific Ocean, *Geophys. Res. Lett.*, 37, 1–5, doi:10.1029/2009GL040999, 2010.

10 Cai, W.-J., Hu, X., Huang, W.-J., Murrell, M. C., Lehrter, J. C., Lohrenz, S. E., Chou, W.-C., Zhai, W., Hollibaugh, J. T., Wang, Y., Zhao, P., Guo, X., Gundersen, K., Dai, M., and Gong, G.-C.: Acidification of subsurface coastal waters enhanced by eutrophication, *Nature Geosci.*, 4, 766–770, 2011.

Caldeira, K. and Wickett, M. E.: Anthropogenic carbon and ocean pH, *Nature*, 425, 365 pp., 2003.

15 Chierici, M. and Fransson, A.: Calcium carbonate saturation in the surface water of the Arctic Ocean: undersaturation in freshwater influenced shelves, *Biogeosciences*, 6, 2421–2431, doi:10.5194/bg-6-2421-2009, 2009.

Cooley, S. R. and Doney, S. C.: Anticipating ocean acidification's economic consequences for commercial fisheries, *Environ. Res. Lett.*, 4, 1–8, doi:10.1088/1748-9326/4/2/024007, 2009.

20 Dickson, A. G.: The carbon dioxide system in seawater: equilibrium chemistry and measurements, in: *Guide to best practices for ocean acidification research and data reporting*, edited by: Riebesell, U., Fabry, V. J., Hansson, L., and Gattuso, J.-P., Publications Office of the European Union, Luxembourg, 260 pp., 2010.

Dierssen, H., Smith, R. C., and Vernet, M.: Glacial meltwater dynamics in coastal waters west of the Antarctic peninsula, *Proceedings of the National Academy of Sciences of the United States of America*, 99, 1790–1795, 2002.

25 Doney, S. C., Fabry, V. J., Feely, R. A., and Kleypas, J. A.: Ocean Acidification: The Other CO₂ Problem, *Ann. Rev. Mar. Sci.*, 1, 169–192, 2009.

Dore, J. E., Lukas, R., Sadler, D. W., Church, M. J., and Karl, D. M.: Physical and biogeochemical modulation of ocean acidification in the central North Pacific, *Proc. Natl. Acad. Sci. USA*, 106, 12235–12240, 2009.

30 Evans, W. and Mathis, J. T.: The Gulf of Alaska coastal ocean as an atmospheric CO₂ sink, *Contin. Shelf Res.*, 65, 52–63, doi:10.1016/j.csr.2013.06.013, 2013

Calcium carbonate corrosivity in an Alaskan inland sea

W. Evans et al.

Title Page

Abstract

Introduction

Conclusions

References

Tables

Figures

◀

▶

◀

▶

Back

Close

Full Screen / Esc

Printer-friendly Version

Interactive Discussion



Evans, W., Hales, B., and Strutton, P. G.: $p\text{CO}_2$ distributions and air-water CO_2 fluxes in the Columbia River estuary, *Estuarine, Coast. Shelf Sci.*, 117, 260–272, doi:10.1016/j.ecss.2012.1012.1003, 2013a.

Evans, W., Mathis, J. T., Winsor, P., Whittedge, T., and Statscewich, H.: A regression modeling approach for studying carbonate saturation states on the northern Gulf of Alaska shelf, *J. Geophys. Res.*, 118, doi:10.1029/2012JC008246, 2013b.

Fabry, V. J., Seibel, B. A., Feely, R. A., and Orr, J. C.: Impacts of ocean acidification on marine fauna and ecosystem processes, *ICES J. Mar. Sci.*, 65, 414–432, 2008.

Feely, R. A., Sabine, C. L., Lee, K., Berelson, W., Kleyvas, J., Fabry, V. J., and Millero, F. J.: Impact of Anthropogenic CO_2 on the CaCO_3 System in the Oceans, *Science*, 305, 362–366, 2004.

Feely, R. A., Sabine, C. L., Hernandez-Ayon, M., Ianson, D., and Hales, B.: Evidence for Upwelling of Corrosive “Acidified” Water onto the Continental Shelf, *Science*, 320, 1490–1492, 2008.

Feely, R. A., Doney, S. C., and Cooley, S. R.: Ocean Acidification: Present Conditions and Future Changes in a High- CO_2 World, *Oceanography*, 22, 36–47, 2009.

Feely, R. A., Alin, S. R., Newton, J., Sabine, C. L., Warner, M., Devol, A., Krembs, C., and Maloy, C.: The combined effects of ocean acidification, mixing, and respiration on pH and carbonate saturation in an urbanized estuary, *Estuarine, Coast. Shelf Sci.*, 88, 442–449, 2010.

Feely, R. A., Klinger, T., Newton, J. A., and Chadset, M.: Scientific Summary of Ocean Acidification in Washington State Marine Waters, 2012.

Gardner, A. S., Moholdt, G., Cogley, J. G., Wouters, B., Arendt, A. A., Wahr, J., Berthier, E., Hock, R., Pfeffer, W. T., Kaser, G., Ligtenberg, S. R. M., Bolch, T., Sharp, M. J., Hagen, J. O., van den Broeke, M. R., and Paul, F.: A Reconciled Estimate of Glacier Contributions to Sea Level Rise: 2003 to 2009, *Science*, 340, 852–857, 2013.

Gay III, S. M. and Vaughan, S. L.: Seasonal hydrography and tidal currents of bays and fjords in Prince William Sound, Alaska, *Fisheries Oceanography*, 10, 159–193, 2001.

Halverson, M. J., Bélanger, C., and Gay III, S. M.: Seasonal transport variations in the straits connecting Prince William Sound to the Gulf of Alaska, *Contin. Shelf Res.*, 63, S63–S78, 2012a.

Halverson, M. J., Ohlmann, J. C., Johnson, M. A., and Pegau, W. S.: Disruption of a cyclonic eddy circulation by wind stress in Prince William Sound, Alaska, *Contin. Shelf Res.*, 63, S13–S25, 2012b.

Calcium carbonate corrosivity in an Alaskan inland sea

W. Evans et al.

Title Page

Abstract

Introduction

Conclusions

References

Tables

Figures

◀

▶

◀

▶

Back

Close

Full Screen / Esc

Printer-friendly Version

Interactive Discussion



- Harris, K. E., Degrandpre, M. D., and Hales, B.: Aragonite Saturation States in a Coastal Upwelling Zone, *Geophys. Res. Lett.*, 40, 2720–2725, 2012.
- Harris, K. E., Degrandpre, M. D., and Hales, B.: Aragonite saturation state dynamics in a coastal upwelling zone, *Geophys. Res. Lett.*, 40, 2720–2725, doi:10.1002/grl.50460, 2013.
- 5 Hood, E., Fellman, J., Spencer, R. G. M., Hernes, P. J., Edwards, R., D'Amore, D., and Scott, D.: Glaciers as a source of ancient and labile organic matter to the marine environment, *Nature*, 464, 1044–1047, 2009.
- Larsen, C. F., Motyka, R. J., Arendt, A. A., Echelmeyer, K. A., and Geissler, P. E.: Glacier changes in southeast Alaska and northwest British Columbia and contribution to sea level rise, *J. Geophys. Res.*, 112, doi:10.1029/2006JF000586, 2007.
- 10 Leinweber, A. and Gruber, N.: Variability and trends of ocean acidification in the Southern California Current System: A time series from Santa Monica Bay, *J. Geophys. Res.*, 118, doi:10.1002/jgrc.20259, 2013.
- Lueker, T. J., Dickson, A. G., and Keeling, R. F.: Ocean $p\text{CO}_2$ calculated from dissolved inorganic carbon, alkalinity, and equations for K_1 and K_2 : validation based on laboratory measurements of CO_2 in gas and seawater at equilibrium, *Mar. Chem.*, 70, 105–119, 2000.
- Mathis, J. T., Cross, J. N., and Bates, N. R.: The role of ocean acidification in systemic carbonate mineral suppression in the Bering Sea, *Geophys. Res. Lett.*, 38, doi:10.1029/2011GL048884, 2011a.
- 20 Mathis, J. T., Cross, J. N., and Bates, N. R.: Coupling primary production and terrestrial runoff to ocean acidification and carbonate mineral suppression in the eastern Bering Sea, *J. Geophys. Res.*, 116, doi:10.1029/2010JC006453, 2011b.
- Mathis, J. T., Cross, J. N., Monacci, N., Feely, R. A., and Stabeno, P. J.: Evidence of prolonged aragonite undersaturations in the bottom waters of the southern Bering Sea shelf from autonomous sensors, *Deep-Sea Res. II*, in press, 2013.
- 25 Mathis, J. T., Cooley, S. R., Lucey, N., Hauri, C., Ekstrom, J., Hurst, T., Colt, S., Evans, W., Cross, J. N., Reisdorph, S., and Feely, R. A.: Ocean Acidification Risk Assessment for Alaska's Fishery Sector, *Contin. Shelf Res.*, in preparation, 2014a.
- Mathis, J. T., Evans, W., Cross, J. N., and Stockwell, D. A.: Physical and Biogeochemical Controllers of Ocean Acidification in the Northern Gulf of Alaska, *J. Geophys. Res.*, in preparation, 2014b.
- 30

Calcium carbonate corrosivity in an Alaskan inland sea

W. Evans et al.

Title Page

Abstract

Introduction

Conclusions

References

Tables

Figures

◀

▶

◀

▶

Back

Close

Full Screen / Esc

Printer-friendly Version

Interactive Discussion



- Miller, L. A., Papakyriakou, T. N., Collins, R. E., Deming, J. W., Ehn, J. K., Macdonald, R. W., Mucci, A., Owens, O., Raudsepp, M., and Sutherland, N.: Carbon dynamics in sea ice: A winter flux time series, *J. Geophys. Res.*, 116, doi:10.1029/2009JC006058, 2011.
- 5 Millero, F. J.: The Marine Inorganic Carbon Cycle, *Chem. Rev.*, 107, 308–341, 2007.
- Mortensen, J., Bendtsen, J., Motyka, R. J., Lennert, K., Truffer, M., Fahnestock, M., and Rysgaard, S.: On the seasonal freshwater stratification in the proximity of fast-flowing tidewater outlet glaciers in a sub-Arctic sill fjord, *J. Geophys. Res.*, 118, 1382–1395, 2013.
- 10 Motyka, R. J., Hunter, L., Echelmeyer, K. A., and Conner, C.: Submarine melting at the terminus of a temperate tidewater glacier, LeConte Glacier, Alaska, USA, *Ann. Glaciol.*, 36, 57–65, 2003.
- Musgrave, D. L., Halverson, M. J., and Pegau, W. S.: Seasonal surface circulation, temperature, and salinity in Prince William Sound, Alaska, *Contin. Shelf Res.*, 53, 20–29, 2013.
- Neal, E. G., Hood, E., and Smikrud, K.: Contribution of glacier runoff to freshwater discharge into the Gulf of Alaska, *Geophys. Res. Lett.*, 37, doi:10.1029/2010GL042385, 2010.
- 15 Niebauer, H. J., Royer, T. C., and Weingartner, T. J.: Circulation of Prince William Sound, Alaska, *J. Geophys. Res.*, 99, 14113–14126, 1994.
- Orr, J. C., Fabry, V. J., Aumont, O., Bopp, L., Doney, S. C., Feely, R. A., Gnanadesikan, A., Gruber, N., Ishida, A., Joos, F., Key, R. M., Lindsay, K., Maier-Reimer, E., Matear, R., Monfray, P., Mouchet, A., Najjar, R. G., Plattner, G.-K., Rodgers, K. B., Sabine, C. L., Sarmiento, J. L., Schlitzer, R., Slater, R. D., Totterdell, I. J., Weirig, M.-F., Yamanaka, Y., and Yool, A.: Anthropogenic ocean acidification over the twenty-first century and its impact on calcifying organisms, *Nature*, 437, 681–686, 2005.
- 20 Pickard, G. L.: Some Oceanographic Characteristics of the Larger Inlets of Southeast Alaska, *Journal of the Fisheries Research Board of Canada*, 24, 1475–1506, 1967.
- Post, A., O’Neel, S., Motyka, R. J., and Streveler, G.: A Complex Relationship Between Calving Glaciers and Climate, *EOS, Transactions, American Geophysical Union*, 92, 305–306, 2011.
- Raven, J., Caldeira, K., Elderfield, H., Hoegh-Guldberg, O., Liss, P. S., Riebesell, U., Shepherd, J., Turley, C., Watson, A. J., Heap, R., Banes, R., and Quinn, R.: Ocean acidification due to increasing atmospheric carbon dioxide, *The Royal Society*, 2005.
- 30 Ritchie, J. B., Lingle, C. S., Motyka, R. J., and Truffer, M.: Seasonal fluctuations in the advance of a tidewater glacier and potential causes: Hubbard Glacier, Alaska, USA, *J. Glaciol.*, 54, 401–411, 2008.

Calcium carbonate corrosivity in an Alaskan inland sea

W. Evans et al.

Title Page

Abstract

Introduction

Conclusions

References

Tables

Figures

◀

▶

◀

▶

Back

Close

Full Screen / Esc

Printer-friendly Version

Interactive Discussion



- Salisbury, J., Green, M., Hunt, C., and Campbell, J.: Coastal Acidification by Rivers: A Threat to Shellfish?, EOS, Transactions, American Geophysical Union, 89, 513–514, 2008.
- Sarmiento, J. L. and Gruber, N.: Ocean Biogeochemical Dynamics, Princeton University Press, Princeton, 2006.
- 5 Sejr, M. K., Krause-Jensen, D., Rysgaard, S., Sørensen, L. L., Christensen, P. B., and Glud, R. N.: Air-sea flux of CO₂ in arctic coastal waters influenced by glacial melt water and sea ice, Tellus, 63B, 815–822, 2011.
- Shadwick, E. H., Rintoul, S. R., Tilbrook, B., Williams, G. D., Young, N., Fraser, A. D., Marchant, H., Smith, J., and Tamura, T.: Glacier tongue calving reduced dense water formation and enhanced carbon uptake, Geophys. Res. Lett., 40, doi:10.1002/grl.50178, 2013.
- 10 Sundquist, E. T., Plummer, L. N., and Wigley, T. M. L.: Carbon Dioxide in the Ocean Surface: The Homogeneous Buffer Factor, Science, 204, 1203–1205, 1979.
- Takahashi, T., Olafsson, J., Goddard, J. G., Chipman, D. W., and Sutherland, S. C.: Seasonal Variation of CO₂ and Nutrients in the High-Latitude Surface Oceans: a Comparative Study, Global Biogeochemical Cycles, 7, 843–878; doi:810.1029/1093GB02263, 1993.
- 15 van Heuven, S., Pierrot, D., Rae, J. W. B., Lewis, E., and Wallace, D. W. R.: MATLAB Program Developed for CO₂ System Calculations Department of Energy, Oak Ridge, Tennessee, 2011.
- Vaughan, S. L., Moers, C. N. K., and Gay III, S. M.: Physical variability in Prince William Sound during the SEA Study (1994–1998), Fisheries Oceanography, 10, 58–80, 2001.
- Walters, R. A., Josberger, E. G., and Driedger, C. L.: Columbia Bay, Alaska: an “Upside Down” Estuary, Estuarine, Coastal and Shelf Science, 26, 607–617, 1988.
- Weingartner, T.: The Physical Environment of the Gulf of Alaska, in: Long-term Ecological Change in the Northern Gulf of Alaska, edited by: Spies, R. B., Elsevier, Oxford, 589 pp., 2007.
- 25 Whittledge, T., Malloy, S. C., Patton, C. J., and Wirick, C. D.: Automated nutrient analyses in seawater, Brookhaven National Laboratory Technical Report BNL 51398, edited by: Laboratory, B. N., National Technical Information Service, Upton, New York, 1981.
- Yamamoto-Kawai, M., McLaughlin, F. A., Carmack, E. C., Nishino, S., and Shimada, K.: Aragonite Undersaturation in the Arctic Ocean: Effects of Ocean Acidification and Sea Ice Melt, Science, 326, 1098–1100, doi:10.1126/science.1174190, 2009.
- 30

Calcium carbonate corrosivity in an Alaskan inland sea

W. Evans et al.

Table 1. Mean (μ), standard deviation (σ), minimum and maximum values of T, S, TA ($\mu\text{mol kg}^{-1}$), DIC ($\mu\text{mol kg}^{-1}$), TA/DIC, $p\text{CO}_2$ (μatm), pH_T , Ω_{arag} and Ω_{calc} for surface (< 9 m) and deep (> 500 m) samples collected in PWS in May and September. The total number of measurements for each parameter was 744; the number of May surface and deep data was 25 and 7, respectively; the number of September surface and deep data was 54 and 20, respectively.

	T		S		TA		DIC		TA/DIC		$p\text{CO}_2$		pH_T		Ω_{arag}		Ω_{calc}	
	μ	σ	μ	σ	μ	σ	μ	σ	μ	σ	μ	σ	μ	σ	μ	σ	μ	σ
May < 9 m	6.1	1.0	30.9	0.7	2111.8	31.7	1916.8	50.3	1.10	0.02	254	59	8.20	0.09	2.07	0.38	3.30	0.61
May > 500 m	5.4	0.1	32.9	0.2	2222.3	15.7	2158.8	23.0	1.03	0.01	724	168	7.77	0.09	0.86	0.16	1.35	0.25
Sep < 9 m	11.5	1.5	25.5	2.5	1845.5	150.5	1693.3	122.8	1.09	0.02	284	39	8.12	0.06	1.69	0.35	2.73	0.54
Sep > 500 m	5.4	0.2	33.1	0.1	2224.6	24.9	2156.8	28.8	1.03	0.01	695	114	7.79	0.07	0.88	0.13	1.39	0.20
	min	max	min	max	min	max	min	max	min	max	min	max	min	max	min	max	min	max
May < 9 m	3.2	7.4	28.7	31.7	2033.6	2151.0	1790.4	1995.0	1.06	1.15	155	376	8.04	8.37	1.43	2.76	2.30	4.41
May > 500 m	5.3	5.6	32.8	33.1	2212.1	2257.0	2135.0	2198.0	1.01	1.04	602	1067	7.60	7.85	0.58	1.03	0.91	1.63
Sep < 9 m	6.1	13.3	18.7	28.3	1285.2	2068.2	1237.0	1861.7	1.04	1.13	205	401	7.96	8.27	0.60	2.49	1.02	3.99
Sep > 500 m	5.2	5.6	32.9	33.3	2154.8	2258.3	2095.7	2200.5	1.01	1.05	529	948	7.65	7.90	0.65	1.10	1.02	1.74

Title Page

Abstract

Introduction

Conclusions

References

Tables

Figures

⏪

⏩

◀

▶

Back

Close

Full Screen / Esc

Printer-friendly Version

Interactive Discussion



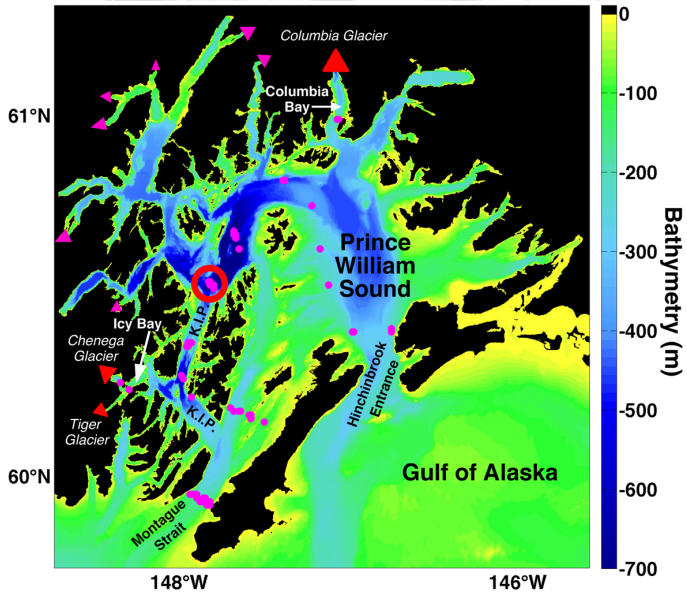
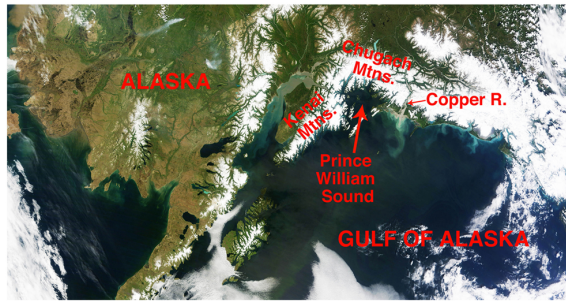


Fig. 1. Caption on next page.

BGD

10, 14887–14922, 2013

Calcium carbonate corrosivity in an Alaskan inland sea

W. Evans et al.

Title Page

Abstract

Introduction

Conclusions

References

Tables

Figures

◀

▶

◀

▶

Back

Close

Full Screen / Esc

Printer-friendly Version

Interactive Discussion



Calcium carbonate corrosivity in an Alaskan inland sea

W. Evans et al.

Title Page

Abstract

Introduction

Conclusions

References

Tables

Figures

◀

▶

◀

▶

Back

Close

Full Screen / Esc

Printer-friendly Version

Interactive Discussion



Fig. 1. Top panel is a Moderate Resolution Imaging Spectroradiometer (MODIS) true color image of southern Alaska from spectral data collected aboard the National Aeronautics and Space Administration (NASA) Terra satellite on June 16, 2013. The image was provided by the NASA Earth Observatory (<http://earthobservatory.nasa.gov/IOTD/view.php?id=81416&src=eoaiotd>), and shows a cloud-free day over southern Alaska with Prince William Sound (PWS) and the adjacent Gulf of Alaska (GOA) visible from space. Labeled geological features relevant to this study are: the Chugach and Kenai Mountain ranges on the north and west side of PWS, respectively, and the Copper River. Lower panel is bathymetry (color-bar; m) of PWS with the locations of hydro-casts marked where dissolved inorganic carbon (DIC) and total alkalinity (TA) measurements were collected (magenta dots). Hinchinbrook Entrance and Montague Strait are labeled, as these are the major connections between PWS and the GOA. Knight Island Passage (K.I.P.) is the north-south oriented channel in the western portion of PWS. Icy Bay and Columbia Bay are marked because these fjords were sampled for the reason that they contain tidewater glaciers. The glaciers in these fjords are marked by red triangles, and other tidewater glaciers in PWS are marked by magenta triangles. Bathymetry data are from a digital elevation model (DEM) provided by the National Oceanic and Atmospheric Administration (NOAA) National Geophysical Data Center (NGDC; <http://www.ngdc.noaa.gov/mgg/coastal/>). The red circle delineates the single station (PWS2) that was sampled during every survey of PWS from 2009 through 2012.

Calcium carbonate
corrosivity in an
Alaskan inland sea

W. Evans et al.

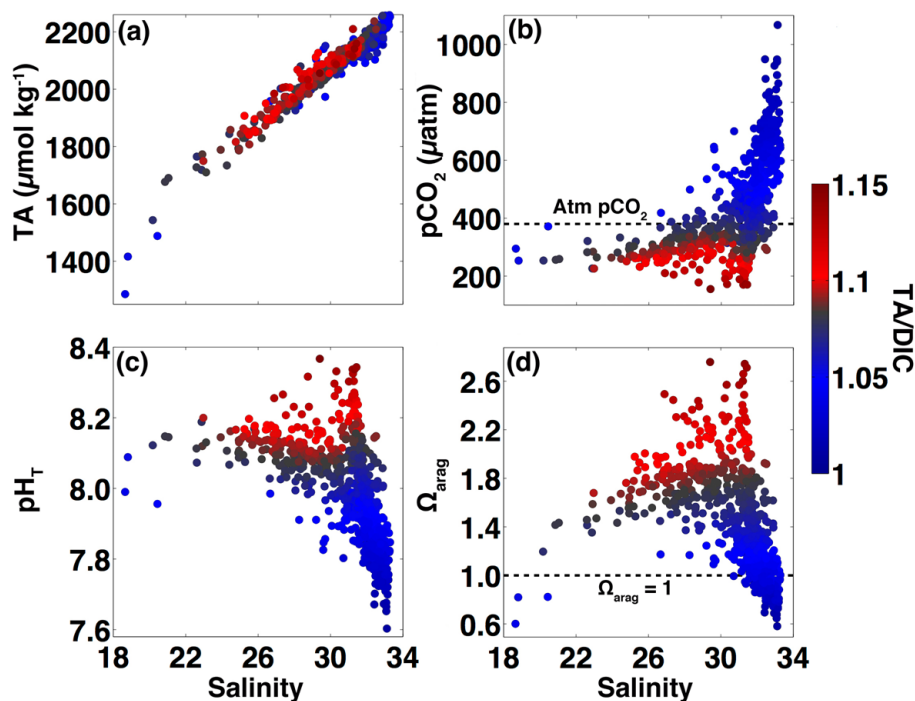


Fig. 2. TA (a; $\mu\text{mol kg}^{-1}$), $p\text{CO}_2$ (b; μatm), pH_T (c), and Ω_{arag} (d) as a function of salinity and TA/DIC ratio from all May and September measurements collected within PWS between 2009 and 2012. The dashed horizontal line in panel (b) is the September 2012 atmospheric $p\text{CO}_2$ in PWS estimated following Evans and Mathis (2013; 380 μatm), and the dashed horizontal line in panel (d) is the $\Omega_{\text{arag}} = 1$ level where below which dissolution of aragonite will occur.

Title Page

Abstract

Introduction

Conclusions

References

Tables

Figures

◀

▶

◀

▶

Back

Close

Full Screen / Esc

Printer-friendly Version

Interactive Discussion

Calcium carbonate corrosivity in an Alaskan inland sea

W. Evans et al.

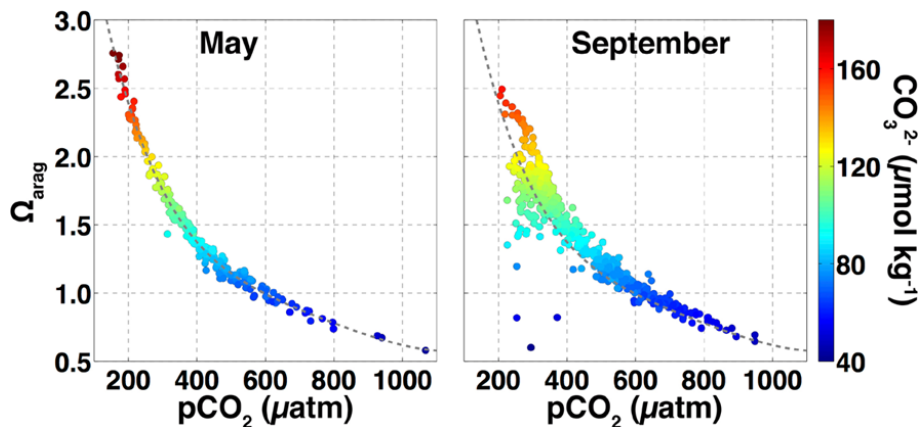


Fig. 3. May (left) and September (right) Ω_{arag} as a function of $p\text{CO}_2$ (μatm) and CO_3^{2-} ($\mu\text{mol kg}^{-1}$). The dashed gray line is a 5th order polynomial fit to the May data. September data fall off the May fit at $p\text{CO}_2 < 600 \mu\text{atm}$; either values are below the fit with low Ω_{arag} and depleted in CO_3^{2-} for a given $p\text{CO}_2$, or values are above the fit with high $p\text{CO}_2$ for a given Ω_{arag} and CO_3^{2-} .

Title Page

Abstract

Introduction

Conclusions

References

Tables

Figures

◀

▶

◀

▶

Back

Close

Full Screen / Esc

Printer-friendly Version

Interactive Discussion



Calcium carbonate
corrosivity in an
Alaskan inland sea

W. Evans et al.

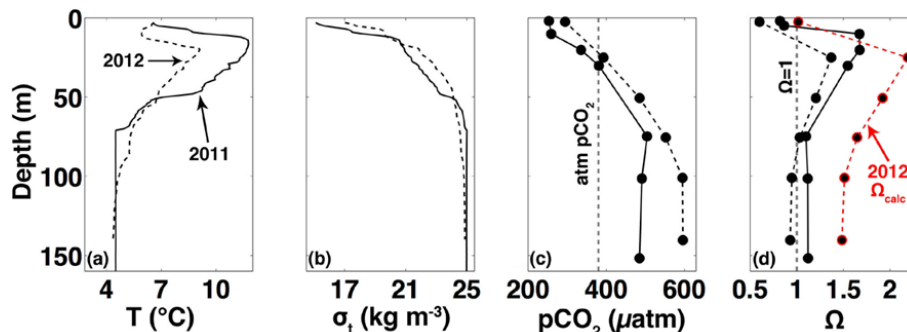


Fig. 4. Depth profiles from Icy Bay (Fig. 1) collected during September in 2011 (solid lines) and 2012 (dashed lines) of temperature (**a**; °C), σ_t (**b**; kg m⁻³), pH_T (**c**), and Ω (**d**). The gray dashed line in panel d denotes the $\Omega = 1$ level where below which calcium carbonate dissolution will occur. Panel d shows both Ω_{arag} (black) and Ω_{calc} (red); nearly corrosive surface levels of Ω_{calc} (1.02) were seen for the first time in the GOA at this site in September 2012.

Title Page

Abstract

Introduction

Conclusions

References

Tables

Figures

◀

▶

◀

▶

Back

Close

Full Screen / Esc

Printer-friendly Version

Interactive Discussion



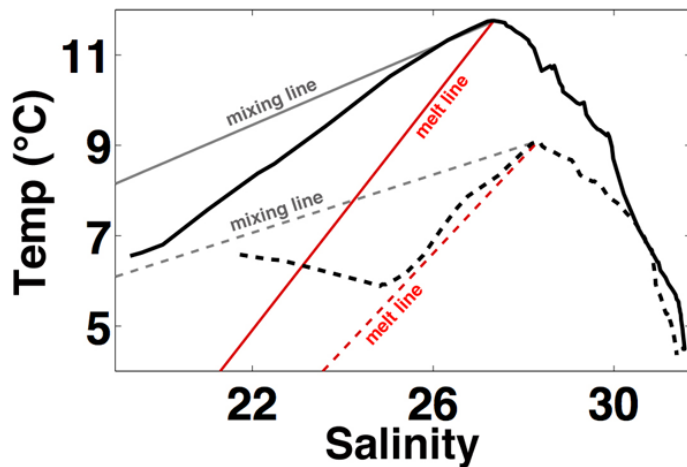


Fig. 5. Temperature (°C)-salinity diagram for September 2011 (black solid line) and September 2012 (black dashed line) profiles in Icy Bay (Fig. 1). The solid and dashed gray lines are mixing lines between source waters estimated from Fig. 4, and freshwater at 0°C, with solid and dashed lines marking 2011 and 2012 data, respectively. The solid and dashed red lines are mixing lines that describe ice melting in seawater, following Walters et al. (1988), with the 2011 and 2012 source water characteristics, respectively.

**Calcium carbonate
corrosivity in an
Alaskan inland sea**

W. Evans et al.

Title Page

Abstract

Introduction

Conclusions

References

Tables

Figures

◀

▶

◀

▶

Back

Close

Full Screen / Esc

Printer-friendly Version

Interactive Discussion



BGD

10, 14887–14922, 2013

Calcium carbonate
corrosivity in an
Alaskan inland sea

W. Evans et al.

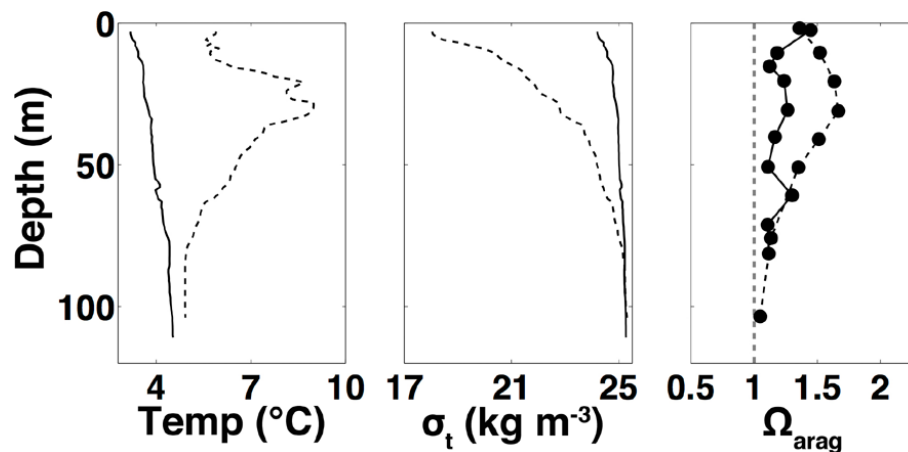


Fig. 6. Depth profiles of temperature (°C; left), σ_t (kg m⁻³; middle) and Ω_{arag} (right) collected in Columbia Bay (Fig. 1) during spring 2012 (solid lines) and autumn 2012 (dashed lines). The vertical gray dashed line in the right panel denotes the $\Omega_{\text{arag}} = 1$ level where below which dissolution of aragonite will occur.

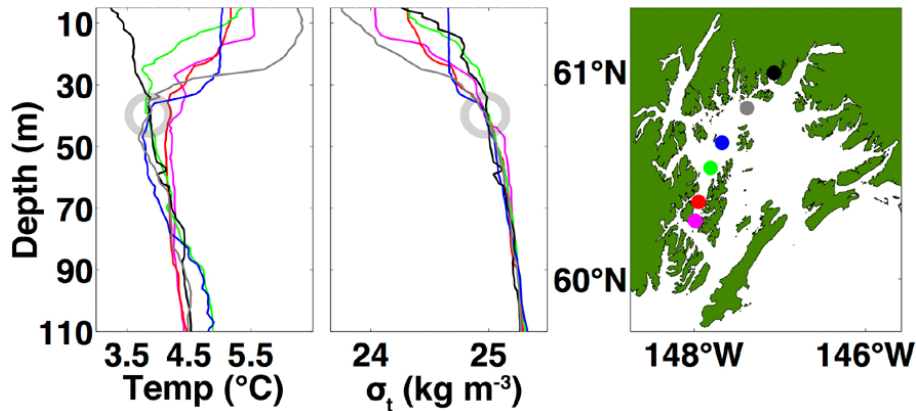


Fig. 7. Spring 2012 depth profiles of temperature ($^{\circ}\text{C}$) and σ_t (kg m^{-3}). The color of the profiles corresponds to the station positions shown on the map. The mode water with T and σ_t characteristics is identified with a gray circle in each panel.

BGD

10, 14887–14922, 2013

Calcium carbonate corrosivity in an Alaskan inland sea

W. Evans et al.

Title Page

Abstract

Introduction

Conclusions

References

Tables

Figures

◀

▶

◀

▶

Back

Close

Full Screen / Esc

Printer-friendly Version

Interactive Discussion



Calcium carbonate
corrosivity in an
Alaskan inland sea

W. Evans et al.

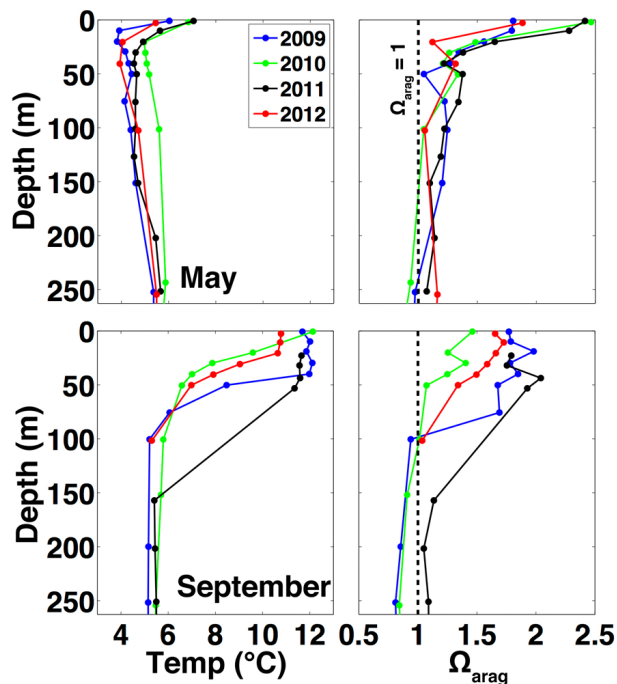


Fig. 8. Temperature ($^{\circ}\text{C}$; left) and Ω_{arag} (right) for K.I.P. station PWS2 (Fig. 1) for spring (top) and autumn (bottom) from 2009 through 2012. The dashed vertical lines in the right panels denote the $\Omega_{\text{arag}} = 1$ level where below which aragonite will dissolve.

Title Page

Abstract

Introduction

Conclusions

References

Tables

Figures

◀

▶

◀

▶

Back

Close

Full Screen / Esc

Printer-friendly Version

Interactive Discussion



BGD

10, 14887–14922, 2013

Calcium carbonate
corrosivity in an
Alaskan inland sea

W. Evans et al.

Title Page

Abstract

Introduction

Conclusions

References

Tables

Figures

◀

▶

◀

▶

Back

Close

Full Screen / Esc

Printer-friendly Version

Interactive Discussion

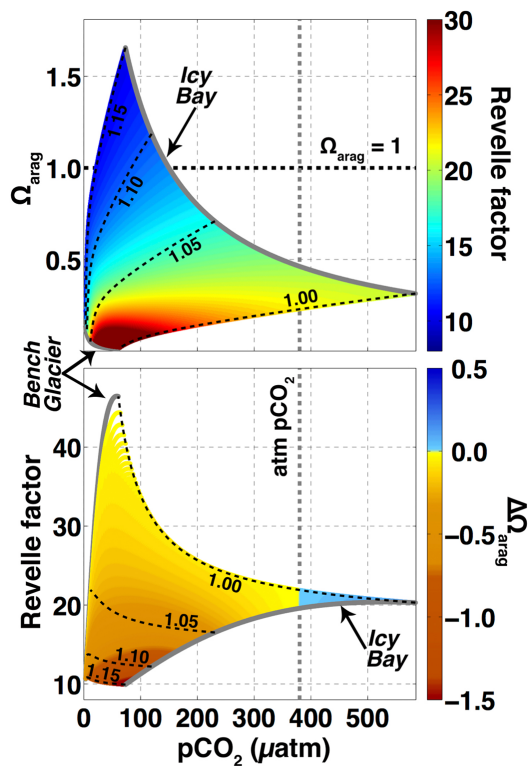


Fig. 9. Caption on next page.

Calcium carbonate corrosivity in an Alaskan inland sea

W. Evans et al.

Title Page

Abstract

Introduction

Conclusions

References

Tables

Figures

◀

▶

◀

▶

Back

Close

Full Screen / Esc

Printer-friendly Version

Interactive Discussion



Fig. 9. A representation of the positive feedback between the addition of direct glacial melt and the uptake of atmospheric CO_2 on Ω_{arag} . Top panel shows the effect of glacier melt addition and the TA/DIC ratio (1.00 to 1.15) on Ω_{arag} , $p\text{CO}_2$ (μatm) and the Revelle factor for water masses mixed linearly between Icy Bay TA ($1250 \mu\text{mol kg}^{-1}$), S (18) and T (5°C) and Bench Glacier TA ($430 \mu\text{mol kg}^{-1}$), S (0) and T (0°C) at 1 atm. Bench Glacier TA is from Anderson et al. (2000). Icy Bay and Bench Glacier data over the range of TA/DIC ratios are marked with gray lines. The black horizontal dashed line is the $\Omega_{\text{arag}} = 1$ level, below which dissolution of aragonite will occur. The gray vertical dashed line is the September 2012 atmospheric $p\text{CO}_2$ in Prince William Sound estimated following Evans and Mathis (2013; $380 \mu\text{atm}$). Trajectories of constant TA/DIC show different scenarios of increasing Ω_{arag} and $p\text{CO}_2$, and decreasing Revelle factors. The lower panel shows the change in Ω_{arag} ($\Delta\Omega_{\text{arag}}$) that would result from the complete equilibration of the melt plumes with the atmosphere at the $p\text{CO}_2$, DIC and Revelle factor conditions represented by the trajectories shown in the top panel (i.e. lines of TA/DIC are those shown in top panel and not adjusted for air-sea gas exchange). As such, $\Delta\Omega_{\text{arag}}$ is negative in waters gaining DIC and being acidified, and positive in waters losing DIC via air-sea gas exchange. The most negative $\Delta\Omega_{\text{arag}}$ values are in buffered plume water (Revelle factor < 15) with high TA/DIC ratios due to $p\text{CO}_2$ levels well below saturation with the atmosphere and saturated Ω_{arag} values. Weakly buffered, low- $p\text{CO}_2$ melt water already have Ω_{arag} values near zero, so CO_2 uptake from the atmosphere will have little effect.